Fast Algorithm for Nonsubsampled Contourlet Transform

YAN Chun-Man[1] GUO Bao-Long[2] YI Meng[2]

Abstract The multiscale geometric analysis (MGA) has been recognized as an effective strategy for image processing. As one of the discrete tools of MGA, the nonsubsampled contourlet transform (NSCT) has been widely used for image denoising, image fusion, image enhancement, feature extraction and so on. However, the processing performance is limited due to its high redundancy, and leading to an intensive computational efficiency. Therefore, its fast algorithm is desired in practice. In this paper, we adopt an optimized directional filter bank (DFB) and embed it into the NSCT to significantly accelerate the computational speed while keeping slight loss of the reconstructed performance. Experimental results show that the reconstructed image quality can satisfy the human visual system. Moreover, the improved NSCT has a speed about several times than that of the traditional one. Experimental results on image denoising also validate the feasibility and efficiency of the proposed method.

Key words Directional filter bank (DFB), fast algorithm, multiscale geometric analysis (MGA), nonsubsampled contourlet transform (NSCT)

Citation Yan Chun-Man, Guo Bao-Long, Yi Meng. Fast algorithm for nonsubsampled contourlet transform. *Acta Automatica Sinica*, 2014, **40**(4): 757−762

DOI 10.3724/SP.J.1004.2014.00757

Wavelets have found wide applications in signal processing due to the time-frequency localization and multiscale decomposition property. Wavelets are well adapted to abrupt changes or singularities of signal; unfortunately, they are not the most optimal and best sparse representation for a function in high dimension. With the developments of computational harmonic analysis, computer vision, pattern recognition, and statistics, a novel multiscale geometric analysis (MGA) theory was proposed to capture the intrinsic geometrical structure of pictorial information. With these MGA tools, one can achieve optimal representation for high dimensional function. The MGA tools with multiscale, multiresolution, and multidirection decomposition are more beneficial for image processing, which can achieve appealing performance over wavelets. Over the past few years, it has been proved that they are quite useful and have been successfully applied in many signal processing fields.

Generally, the MGA methods can be categorized into two classes: adaptive methods and non-adaptive methods. The principle of the adaptive methods is that the transform basis changes according to the contents of image to be processed. These methods include brushlet[1], bandelet[2], directionlet[3], and so on. Fundamentally, the adaptive methods require some prior knowledge of image (e.g., edge detection). Therefore, for an image with complex structures and rich textures, the obtained performance by this family of methods is not as good as wavelets. The representatives of the non-adaptive methods include ridgelet[4], curvelet[5−7], and contourlet[8−9]. The ridgelet can achieve optimal representation for a function with linear singularity in high dimensional size; Nonetheless, its sparse representation performance is just as wavelets for a function with curve singularity. Based on the ridgelet, the curvelet was proposed by Candès et al.[5−7]. Because of the procedure of subband decomposition, smooth partitioning, renormalization, and ridgelet analysis, curvelet is very complex for numerical application. To handle this adverse influence, a fast discrete curvelet transform was later presented by Candès et al.[7], which is implemented by unequally spaced fast Fourier transform and wrapping-based transform. curvelet can provide anisotropy scaling relation which is a key factor for image sparse representation, and it can achieve high-performance representation of a function with curve singularity. Under the enlightenment of curvelet, Do et al. proposed a "true" image representation method, namely contourlet transform (CT)[8−9], which succeeds to the multidirection and anisotropy of curvelet, and can provide an optimal edge description for images. The contourlet may be seen as the discrete version of curvelet with lower redundancy. However, the original contourlet is not just shift-invariant and may cause pseudo-Gibbs phenomena around singularities. To overcome this problem, the nonsubsampled contourlet transform (NSCT) was suggested by da Cunha et al.[10]. The NSCT is a fully shift-invariant, multiscale, and multidirection expansion for images. Moreover, its iterated structure is easy to construct. With high redundancy, the NSCT is proved to be very useful for many special image processing tasks, such as image denoising[11], image despeckling[12], and image fusion[13−14]. However, its high redundancy consequentially leads to an overloading computational cost. As a result, it is necessary to develop a fast algorithm for the NSCT in practice. Considering that the directional filter bank (DFB) plays a key role in the NSCT, in this paper, we adopt an optimized DFB and embed it into the NSCT to improve its performance. To validate the feasibility and efficiency of the proposed strategy, we first carry out an experiment on image decomposition and reconstruction task. It is experimentally shown that the improved NSCT can obtain a remarkable processing speed by sacrificing a loss of the reconstruction error, while preserving the reconstructed image quality sufficient enough for the human visual system. We further conduct another experiment on image denoising. The experimental results suggest that, with a slight loss of peak signal-to-noise ratio (PSNR) value on average, the processing speed of the improved method is about 7 times faster than that of the traditional one.

Manuscript received January 24, 2012; accepted May 24, 2013
Supported by National Natural Science Foundation of China (61367005, 61162017) and the Fundamental Research Funds for the Universities of Gansu Province
Recommended by Associate Editor DAI Qiong-Hai
1. College of Physics and Electronic Engineering, Northwest Normal University, Lanzhou 730070, China 2. Institute of Intelligent Control and Image Engineering, Xidian University, Xi′an 710071, China

1 Structure of the directional filter bank

The original construction of the DFB was proposed by Bamberger and Smith in 1992[15], which employs quincunx filter banks (QFB) and the input image is required to modulate. To simplify and improve the frequency partition, Do and Vetterli proposed an improved DFB[8−9], in which the QFB is also used and an ideal frequency partition is obtained without modulating the input image. As the key factor of the DFB, the QFB uses diamond filter pair and fan filter pair for frequency partition, where the first one divides the frequency into low and high subbands, while the second one obtains vertical and horizontal subbands for directional partition. We can obtain one filter pair from the other by modulating the filter by π in either the ω_0 or ω_1 frequency variable. Thus, only one filter design is needed in practice.

The DFB is efficiently implemented via an ℓ-level binary tree decomposition, which leads to 2^ℓ subbands with wedge-shaped frequency partition. To illustrate the frequency partitioning, Fig. 1 shows a four-channel DFB, where Fig. 1 (a) demonstrates the first two levels of the DFB, the black regions represent the ideal frequency supports of the filter, Q_0 and Q_1 are sampling matrices[8−9].

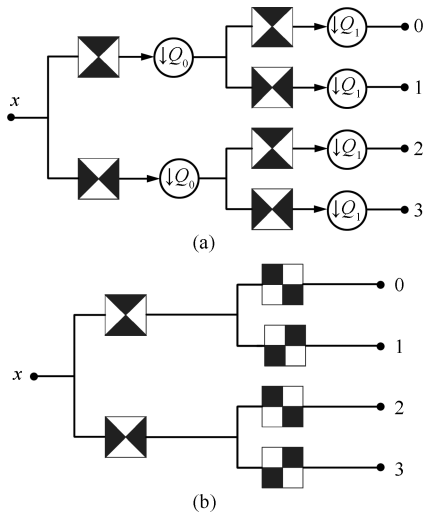

Fig. 1 Four-channel DFB ((a) The block building of the first two stages; (b) Equivalent block building of (a))

For the four directional frequency partitions, we can exchange the resampling operator at the first stage and the fan filter at the second stage by using multirate identities, and then we obtain the equivalent quadrant filter at the second stage, as shown in Fig. 1 (b).

For an ℓ-level tree structured DFB, it can be equivalently viewed as a 2^ℓ parallel channel filter bank by the identities of multirate system as shown in Fig. 2, where H_k and G_k are the analysis filter and the synthesis filter respectively, and S_k is the resampling matrix. For S_k, we use S_k^ℓ to denote a diagonal matrix at the ℓ-th level, which is given by (1). According to the directional angle range, S_k^ℓ is divided into two forms, i.e., the horizontal ($-45^\circ \sim 45^\circ$, $0 \le k < 2^{\ell-1}$) and the vertical ($45^\circ \sim 135^\circ$, $2^{\ell-1} \le k < 2^\ell$) directions, respectively.

$$S_k^\ell = \begin{cases} \begin{bmatrix} 2^{\ell-1} & 0 \\ 0 & 2 \end{bmatrix}, & \text{for } 0 \le k < 2^{\ell-1} \\ \begin{bmatrix} 2 & 0 \\ 0 & 2^{\ell-1} \end{bmatrix}, & \text{for } 2^{\ell-1} \le k < 2^\ell \end{cases} \tag{1}$$

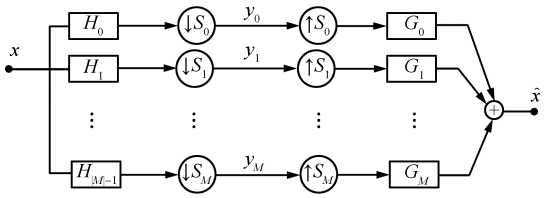

Fig. 2 The equivalent multi-channel system of DFB

2 Optimal design of the directional filter bank for NSCT

The contourlet expansion, associated with multiscale, multidirection, and anisotropy, uses contour segment like function to approximate a natural image at multiple scales and multiple directions. There are two filter banks used in contourlet transform, wherein the Laplacian pyramid (LP) filter bank is employed to decompose the image into multiscale components at the first stage; and the directional filter bank (DFB) is used to obtain directional subbands at high scale at the next stage. Therefore, the contourlet expansion is also called pyramidal directional filter bank (PDFB). In the process of decomposition and reconstruction, because downsampling and upsampling operations may cause spectral aliasing, so it is not shift-invariant. By contrast, the NSCT uses the nonsubsampled Laplacian pyramid filter bank (NSPFB) and the nonsubsampled directional filter bank (NSDFB) to replace the original LP and DFB. In such a way, the NSCT can obtain shift-invariability. Accordingly, the NSCT employs a double filter bank structure, i.e., the NSPFB is used for multiscale decomposition, which is followed by NSDFB for directional subbands at high scale, and an iterative process is performed at the coarse scale. This can obtain multiscale and multidirection decomposition for an image. Therefore, to capture the geometrical structure of an image, an optimal design of the DFB for NSCT is very important. As aforementioned in Section 1, we can know that the QFB is key to a DFB. Inspired by this cue, we mainly focus on how to design an optimal QFB in this paper.

To achieve a high performance, the QFB should have the ability of perfect reconstruction (PR), high coding gain, good frequency selectivity, certain prescribed vanishing moments, and linear-phase. The PR property ensures a high peak signal-to-noise ratio (PSNR) of the reconstructed image. The linear-phase property helps to avoid phase distortion. The presence of vanishing moments benefits to reduce the number of nonzero coefficients in the highpass subbands and get smoother synthesis basis functions. While good frequency selectivity is useful to minimize aliasing in the subband signals[16].

To design nonseparable two-dimensional filter banks with the aforementioned properties, lifting scheme[17−18] should be one of the valuable options. This reversible integer-to-integer transform is meaningful for image processing and helps to improve the processing speed. The PR condition can naturally be satisfied via its parameterization, and the linear-phase condition can be imposed with

relative ease. Thus, unlike the traditional structure, we adopt the lifting scheme proposed in [16] and summarize it in what follows. The structure of this scheme is shown in Fig. 3, where $x[\boldsymbol{n}]$ is the input signal, $x_r[\boldsymbol{n}]$ is the reconstructed signal, $y_0[\boldsymbol{n}]$ and $y_1[\boldsymbol{n}]$ are the subbands of $x[\boldsymbol{n}]$, and $A_k(\boldsymbol{z})$ is the lifting filter.

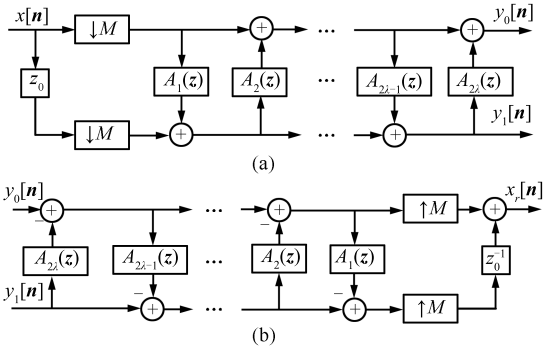

Fig. 3 The structure of the lifting scheme of a QFB with 2λ lifting steps ((a) Analysis filters; (b) Synthesis filters)

The design problem of a QFB involves two parts: the analysis filters and the synthesis filters. For the lifting scheme, given the coefficients of the lifting filter $\{A_k(\boldsymbol{z})\}$, the transfer function of the analysis filter can be calculated. Correspondingly, the transfer function of the synthesis filters can be obtained by the PR condition, which can be calculated from the function $G_k(\boldsymbol{z}) = (-1)^{1-k} z_0^{-1} H_{1-k}(-\boldsymbol{z})$. As a consequence, the major task of filter bank design is to construct the coefficients of the lifting filter $\{A_k(\boldsymbol{z})\}$. For the purpose, we need to parameterize the QFB and only consider the analysis side of the filter bank, which is specified as follows.

According to the lifting property, the need for additional constraints during optimization for PR and linear phase can be eliminated. Thus, we only discuss the two important constraint conditions: frequency response and vanishing moments.

1) Frequency response

Let $\boldsymbol{x}$ be a vector consisting of all the independent coefficients of lifting filter $\{A_k\}$, which takes the form of $\boldsymbol{x} = \left[\begin{array}{cccc} a_1^{\mathrm{T}} & a_2^{\mathrm{T}} & \cdots & a_{2\lambda}^{\mathrm{T}} \end{array}\right]^{\mathrm{T}}$. The number of independent coefficients in $\{A_k\}$ is $2l_{k,0}l_{k,1}$, and the frequency responses of the analysis filters can be defined as (2):

$$\left[\begin{array}{c} \hat{h}_0(\boldsymbol{\omega}) \\ \hat{h}_1(\boldsymbol{\omega}) \end{array}\right] = \left(\prod_{k=1}^{\lambda}\left(\left[\begin{array}{cc} 1 & \mathrm{e}^{-\mathrm{j}\omega_0}\boldsymbol{a}_{2k}^{\mathrm{T}}\boldsymbol{V}_{2k} \\ 0 & 1 \end{array}\right] \times \left[\begin{array}{cc} 1 & 0 \\ \mathrm{e}^{\mathrm{j}\omega_0}\boldsymbol{a}_{2k-1}^{\mathrm{T}}\boldsymbol{V}_{2k-1} & 1 \end{array}\right]\right)\right)\left[\begin{array}{c} 1 \\ \mathrm{e}^{\mathrm{j}\omega_0} \end{array}\right] \quad (2)$$

where $\boldsymbol{V}_{2k}$ is a vector with $2l_{2k,0}l_{2k,1}$ elements, and $\boldsymbol{V}_{2k-1}$ is a vector with $2l_{2k-1,0}l_{2k-1,1}$ elements. The n-th element in the two vectors are respectively given by:

$$\boldsymbol{V}_{2k}[\boldsymbol{n}] = 2\cos\left[\omega_0(n_0+n_1-1)+\omega_1(n_0-n_1)\right] \quad (3)$$

$$\boldsymbol{V}_{2k-1}[\boldsymbol{n}] = 2\cos\left[\omega_0(n_0+n_1+1)+\omega_1(n_0-n_1)\right] \quad (4)$$

with $\boldsymbol{n} = \left[\begin{array}{cc} n_0 & n_1 \end{array}\right]^{\mathrm{T}}$, and $n_0, n_1 \in \mathbf{Z}$.

By expanding the above equation, the frequency responses of the analysis filter can be viewed as a polynomial of $\boldsymbol{x}$, the order of which depends on the number of lifting steps.

2) Vanishing moments

For a QFB, the number of vanishing moments is equivalent to the order of zero at $\left[\begin{array}{cc} 0 & 0 \end{array}\right]^{\mathrm{T}}$ or $\left[\begin{array}{cc} \pi & \pi \end{array}\right]^{\mathrm{T}}$ in the frequency response, respectively. For a linear-phase filter H with group delay $\boldsymbol{d} \in \mathbf{Z}^2$, its frequency response is defined as $\hat{h}(\boldsymbol{\omega})$ and its signed amplitude response as $\hat{h}_a(\boldsymbol{\omega})$, then the m-th order partial derivative of $\hat{h}_a(\boldsymbol{\omega})$ in the Fourier domain is then given by (5):

$$\frac{\partial^{m_0+m_1}\hat{h}_a(\boldsymbol{\omega})}{\partial\omega_0^{m_0}\partial\omega_1^{m_1}} = \begin{cases} \sum\limits_{\boldsymbol{n}\in\mathbf{Z}^2} h[\boldsymbol{n}](\boldsymbol{n}-\boldsymbol{d})^{\boldsymbol{m}}\cos\left[\boldsymbol{\omega}^{\mathrm{T}}(\boldsymbol{n}-\boldsymbol{d})\right], & \text{for } |\boldsymbol{m}| \in \mathbf{Z}_{\text{even}} \\ -\sum\limits_{\boldsymbol{n}\in\mathbf{Z}^2} h[\boldsymbol{n}](\boldsymbol{n}-\boldsymbol{d})^{\boldsymbol{m}}\sin\left[\boldsymbol{\omega}^{\mathrm{T}}(\boldsymbol{n}-\boldsymbol{d})\right], & \text{otherwise} \end{cases} \quad (5)$$

where $\boldsymbol{m} = \left[\begin{array}{cc} m_0 & m_1 \end{array}\right]^{\mathrm{T}}$. From (5), when $|\boldsymbol{m}| \in \mathbf{Z}_{\text{even}}$, the m-th order partial derivative is zero at $\left[\begin{array}{cc} 0 & 0 \end{array}\right]^{\mathrm{T}}$ and $\left[\begin{array}{cc} \pi & \pi \end{array}\right]^{\mathrm{T}}$. Therefore, in order to obtain an N-th order zero at $\left[\begin{array}{cc} 0 & 0 \end{array}\right]^{\mathrm{T}}$, the coefficients of the filter only should be satisfied with the following condition:

$$\sum_{n\in\mathbf{Z}^2} h[\boldsymbol{n}](\boldsymbol{n}-\boldsymbol{d})^{\boldsymbol{m}}=0, \text{ for } |\boldsymbol{m}| \in \mathbf{Z}_{\text{even}}, |\boldsymbol{m}| < N \quad (6)$$

Similarly, in order to obtain an N-th order zero at $\left[\begin{array}{cc} \pi & \pi \end{array}\right]^{\mathrm{T}}$, the filter coefficients should satisfy the condition as below:

$$\sum_{\boldsymbol{n}\in\mathbf{Z}^2} (-1)^{|\boldsymbol{n}-\boldsymbol{d}|} h[\boldsymbol{n}](\boldsymbol{n}-\boldsymbol{d})^{\boldsymbol{m}}=0, \text{ for } |\boldsymbol{m}| \in \mathbf{Z}_{\text{even}}, \ |\boldsymbol{m}| < N \quad (7)$$

Since it uses a lifting-based parameterization, the relationships need to be represented in terms of the lifting filter coefficients. For a filter bank with N, $\tilde{N}$ primal and dual vanishing moments, the coefficients of the analysis filter are required to satisfy (8):

$$A\boldsymbol{x} = \boldsymbol{b} \quad (8)$$

Here, we briefly give the example of a filter with two lifting steps. For (8), let $A = \left[\begin{array}{cc} A_1 & 0 \\ 0 & A_2 \end{array}\right]$, $\boldsymbol{x} = \left[\begin{array}{c} \boldsymbol{a}_1 \\ \boldsymbol{a}_2 \end{array}\right]$, $\boldsymbol{b} = \left[\begin{array}{c} \boldsymbol{b}_1 \\ \boldsymbol{b}_2 \end{array}\right]$. The number of equations is $[\tilde{N}/2]^2 + [N/2]^2$. Accordingly, $\boldsymbol{b}_1$ is a vector with $[\tilde{N}/2]^2$ elements, and each element of it takes the form of $-2^{-|\boldsymbol{m}|}$. $\boldsymbol{b}_2$ is a vector with $[N/2]^2$ elements, and each element of it takes the form of $-(-2)^{-|\boldsymbol{m}|-1}$. Let the singular value decomposition (SVD) of A be $A = USV^{\mathrm{T}}$, then all of the solutions to (8) can be parameterized as the following:

$$\boldsymbol{x} = \boldsymbol{x}_s + V_r\boldsymbol{\varphi} \quad (9)$$

where V_r is a matrix composed of the last $(n-r)$ columns of V, and $\boldsymbol{\varphi}$ is an arbitrary $(n-r)$-dimensional vector. Henceforth, $\boldsymbol{\varphi}$ can be used as the design vector.

From the above discussion, the vanishing moment condition is the solution of a system of $[N/2]^2 + [N/2]^2$ linear equations, and the frequency condition is an optimization problem for the coefficients of the lifting filter, which makes it as close as possible to ideal frequency response. In this way, the design objective is to maximize the coding gain G_c subject to a set of constraints, which are chosen to ensure

that the desired vanishing moment and frequency selectivity conditions are met. Since the coding gain G_c can be expressed as a nonlinear function of vector $\boldsymbol{\varphi}$, Suppose that $G = -10\lg G_c$, for a given parameter vector $\boldsymbol{\varphi}$, we should seek a small perturbation $\boldsymbol{\delta}_{\boldsymbol{\varphi}}$ such that $G(\boldsymbol{\varphi}+\boldsymbol{\delta}_{\boldsymbol{\varphi}})$ is reduced with regard to $G(\boldsymbol{\varphi})$. Because $\|\boldsymbol{\delta}_{\boldsymbol{\varphi}}\|$ is small, the linear approximations of $G(\boldsymbol{\varphi}+\boldsymbol{\delta}_{\boldsymbol{\varphi}})$ can be written as (10):

$$G(\boldsymbol{\varphi}+\boldsymbol{\delta}_{\boldsymbol{\varphi}}) = G(\boldsymbol{\varphi}) + \boldsymbol{g}^{\mathrm{T}}\boldsymbol{\delta}_{\boldsymbol{\varphi}} \tag{10}$$

where $\boldsymbol{g}$ is the derivative of G at $\boldsymbol{\varphi}$ point. Then the design task is to search $\boldsymbol{\delta}_{\boldsymbol{\varphi}}$, until $|G(\boldsymbol{\varphi}+\boldsymbol{\delta}_{\boldsymbol{\varphi}}) - G(\boldsymbol{\varphi})|$ becomes less than a predetermined tolerance ε.

To accomplish the design of a filter with two lifting steps, the core optimizing procedure is summarized as below:

Step 1. Calculate A and $\boldsymbol{b}$ from (8), with the frequency constraint, calculate the error of high-pass analysis filter. The error function is given by (11):

$$e_h = \boldsymbol{\varphi}^{\mathrm{T}} H_{\boldsymbol{\varphi}} \boldsymbol{\varphi} + \boldsymbol{\varphi}^{\mathrm{T}} \boldsymbol{s}_{\boldsymbol{\varphi}} + c_{\boldsymbol{\varphi}} \tag{11}$$

Note that the initial value of $\boldsymbol{\varphi}_0$ can be randomly selected.

Step 2. For the k-th iteration, compute $\boldsymbol{g}$ at the point $\boldsymbol{\varphi}_k$, the derivative of $G(\boldsymbol{x})$, calculate $\tilde{H}_k, \tilde{\boldsymbol{s}}_k, \tilde{c}_k$, and minimize $\boldsymbol{g}^{\mathrm{T}}\boldsymbol{\delta}_{\boldsymbol{\varphi}}$, subject to $\|\tilde{H}_k\boldsymbol{\delta}_{\boldsymbol{\phi}} + \tilde{\boldsymbol{s}}_k\| \le \sqrt{\boldsymbol{\delta}_h - \tilde{c}_k}$ and $\|\boldsymbol{\delta}_{\boldsymbol{\phi}}\| \le \beta$. Here β is a given small value which ensures that the solution is within the vicinity of $\boldsymbol{\varphi}_k$, and $\boldsymbol{\delta}_h$ is a predetermined upper bound on the error. Afterward, update $\boldsymbol{\varphi}_{k+1} = \boldsymbol{\varphi}_k + \gamma\boldsymbol{\delta}_{\boldsymbol{\varphi}}$, where γ is step size. Note that it can be set to 1 or other values, which determines the iteration speed.

Step 3. If $|G(\boldsymbol{\varphi}_{k+1}) - G(\boldsymbol{\varphi}_k)| < \varepsilon$, then output $\boldsymbol{\varphi}^* = \boldsymbol{\varphi}_{k+1}$, $\boldsymbol{x}^* = \boldsymbol{x}_s + V_r\boldsymbol{\varphi}^*$, and stop the procedure. Otherwise, goto Step 2 to continue.

It is noticeable that $\boldsymbol{x}^*$ is the desired output containing optimized coefficients of the lifting filter. In the optimizing procedure above, more details and the rest parameters can be referred to [16].

3 Numerical experiment

In this section, to evaluate the effectiveness of the optimized DFB, we embed it into the original NSCT, identify this NSCT as optimized NSCT, and notate it as ONSCT. We compare the original NSCT with our ONSCT under the numerical experiments. We first perform an experiment on image decomposition and reconstruction task, where the optimized DFB and other different DFBs in the NSCT toolbox are respectively applied in the NSCT model. We next carry out an image denoising experiment by combining the Gaussian scale mixtures model to demonstrate the feasibility and the efficiency of the optimized NSCT. All tests are run in Matlab 7.1 on a laptop, with PM 2.13 GHz CPU, single core, and 1 GB DDR2 RAM.

3.1 Image decomposition and reconstruction

In this subsection, the image zoneplate in the NSCT toolbox is used as the test image. The performance is reflected by the reconstructed image quality and the elapsed time taken by the algorithm. We employ three parameters to assess the performance, including mean square error (MSE), peak signal-to-noise ratio (PSNR), and the elapsed time T. Where MSE and PSNR are used as objective measures to indicate the reconstructed image quality, and T is used to reflect the elapsed time of the image decomposition and reconstruction procedure, which indicates the time complexity of special algorithm, the unit of which is second. Table 1 reports the experimental results. For convenient expression, we denote the optimized directional filter bank as ODFB. In Table 1, the left column lists the names of the different directional filter banks, except the ODFB, and all others come from the NSCT toolbox. In our experiment, the pyramid filter bank is followed the default filter "dmaxflat7" of NSCT. For obvious comparison, the assessment values in Table 1 are arranged in ascending order of the PSNR value.

Table 1 Experimental results of image decomposition and reconstruction on image zoneplate by NSCT using different DFB

Name of DFB	T (s)	MSE	PSNR (dB)
kos	3.02	9.89E+003	9.05
qmf2	4.45	7.66E+003	9.30
ko	3.02	8.37E+003	9.63
Haar	2.59	8.78E+003	9.67
lax	14.9	1.53E+003	20.07
sk	5.66	37.99	33.20
ODFB	2.58	2.00E−004	85.12
Dmaxflat6	55.42	9.45E−009	128.38
cd	4.42	1.57E−021	256.18
Dmaxflat7	73.19	6.54E−025	289.98
Dmaxflat5	38.64	2.51E−025	294.13
Dmaxflat4	25.56	1.29E−025	297.02
pkva	49.78	2.79E−026	303.67
dvmlp	7.53	2.24E−026	304.64

From Table 1, we can see that the PSNR values achieved by kos, qmf2, ko, Haar, lax, and sk filters are low, which means poor reconstructed image quality. From filter ODFB to dvmlp, the PSNR values are high and can meet the need of image processing system. Among all these DFBs, the PSNR value of dvmlp is the highest. Although the result achieved by the ODFB is not as high as that of the dvmlp, the time spent by the former is significantly less than that by the latter. It is noticeable that ODFB runs nearly three times as fast as dvmlp, and about 28 times as fast as the default filter Dmaxfat7.

In order to further evaluate the dependability of the ODFB, we compare the subjective quality of the experimental results obtained by NSCT and ONSCT. In this experiment, two test images are used as benchmark: one is image zoneplate and the other is image Barbara. The two images are representative in that both contain plenty of textures and structure information. We select the filter dvmlp to compare ODFB, because its PSNR value is the highest among all the DFBs. Figs. 4 and 5 show the original image and the reconstructed images by two methods, respectively. The whole resultant zoneplate images are shown in Fig. 4. For more detailed comparisons, Fig. 5 shows the local magnified results of image Barbara. As shown in Figs. 4 and 5, there are no obvious differences and unexpected artifacts in the two results by the proposed ONSCT. Moreover, the PSNR value of 85.12 dB achieved by ONSCT means that the reconstructed result is sufficient enough for human visual system.

For an image processing system in practice, the processing speed should be fully considered. That is to say, under the need of the human visual system, we can sacrifice some PSNR values for achieving a real time application. By using the optimized scheme of filter design, we can yield a desirable visual quality of reconstruction while preserving

high processing performance, which is beneficial to practical applications.

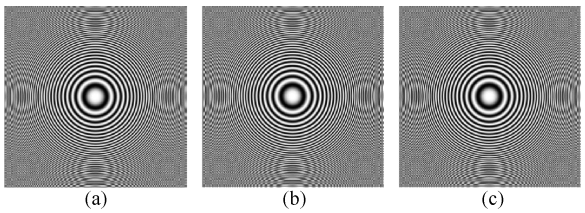

Fig. 4 Comparison of zoneplate image ((a) Original image; (b) Reconstructed result by the original NSCT; (c) Reconstructed result by ONSCT)

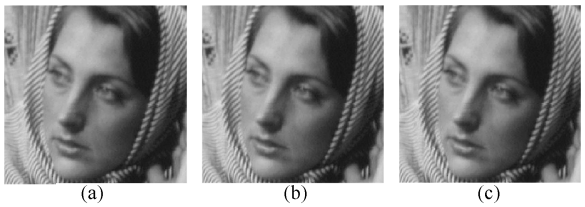

Fig. 5 Comparison of detailed barbara image ((a) Original image; (b) Reconstructed result by the original NSCT; (c) Reconstructed result by ONSCT)

3.2 Image denoising

As we know, the method that combines the NSCT and the Gaussian scale mixtures model (GSM)[11, 19] is an effective way for image denoising. However, the computational cost of this method is considerably intensive. To test the effectiveness of the proposed method that makes a trade-off between denoising performance and computational cost, we apply the proposed ONSCT to assess its performance for image denoising. As the standard test image, image Lena and Barbara are used as the testbed. The original NSCT and the proposed ONSCT are respectively combined with GSM, denoted as NSCT-GSM and ONSCT-GSM, to perform the denoising task. At the LP stage, the pyramid filter bank is selected as in Subsection 3.1 for both NSCT and ONSCT. For NSCT-GSM, we choose the default filter demaxfat7 at the DFB stage. In this test, Gaussian white noises with different variances are added into the original image to produce the noisy images at different noise levels.

The experimental results are shown in Tables 2 and 3. PSNR is also used as objective measurement of image quality, while T is used to represent the elapsed time of denoising procedure, which can reflect the time complexity of the algorithm. σ is the noise variance. As seen, although the average PSNR of the denoised image by ONSCT-GSM is decreased by 0.41 dB and 0.72 dB for image Lena and Barbara, respectively, the average computational time of ONSCT-GSM is significantly decreased by about 7 times as much as that of the NSCT-GSM.

To compare the visual quality of the denoised images, Figs. 6 and 7 show the original image, noisy image, and the denoised image by the two methods, respectively. For careful distinguishing, we give their local magnified results. We can observe that, for additive Gaussian white noise, both methods can produce satisfying denoising results with higher PSNR, fewer artifacts, and well preserved textures. In particular, there are no obvious differences and unexpected artifacts in the denoised images by the ONSCT-GSM method.

Table 2 Image denoising results of image Lena

σ	NSCT-GSM		ONSCT-GSM	
	PSNR	T (s)	PSNR	T (s)
10	35.67	923.8	35.38	113.7
15	33.91	927.2	33.54	114.3
20	32.59	931.9	32.18	115.9
25	31.54	925.1	31.09	115.9
30	30.67	930.9	30.19	120.1
50	28.17	923.9	27.71	121.8
Avg.	32.09	927.12	31.68	116.95

Table 3 Image denoising results of image Barbara

σ	NSCT-GSM		ONSCT-GSM	
	PSNR	T (s)	PSNR	T (s)
10	34.15	933.7	33.65	115.3
15	31.97	922.1	31.31	113.1
20	30.43	932.6	29.67	116.7
25	29.22	923.5	28.41	115.3
30	28.21	931.7	27.36	127.7
50	25.43	925.1	24.67	123.5
Avg.	29.90	928.11	29.18	117.76

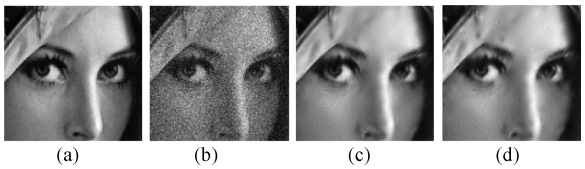

Fig. 6 Comparison of the denoised results on image Lena ($\sigma = 20$) ((a) Original image; (b) Noisy image; (c) Denoised image by NSCT-GSM; (d) Denoised image by ONSCT-GSM)

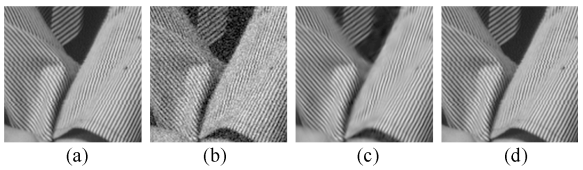

Fig. 7 Comparison of the denoised results on image Barbara ($\sigma = 20$) ((a) Original image; (b) Noisy image; (c) Denoised image by NSCT-GSM; (d) Denoised image by ONSCT-GSM)

4 Conclusion

The NSCT is one of the most effective tools of MGA and can be effectively used for multidimensional signal processing. However, its high computational cost may limit its real time application in practice. In this paper, to achieve a trade-off between the reconstruction quality and computational cost, we adopt a lifting scheme and optimizing step to improve the NSDFB of the NSCT. The experimental results suggest that the processing speed of the improved NSCT significantly outperforms the original one. Furthermore, the image denoising experiments also show that, with a slight loss of PSNR values on average, the proposed method performs at about 7 times faster than the speed of the traditional one, while keeping pleasing visual quality of the resultant image.

In the future work, this improved NSCT also can be naturally extended in other image processing fields, such as image impainting, image restoration, and image fusion.

References

1 Meyer F G, Coifman R R. Brushlets: a tool for directional image analysis and image compression. *Applied and Computational Harmonic Analysis*, 1997, **4**(2): 147−187

2 Le Pennec E, Mallat S. Sparse geometric image representations with Bandelets. *IEEE Transactions on Image Processing*, 2005, **14**(4): 423−438

3 Velisavljevic V, Beferull-Lozano B, Vetterli M, Dragotti P L. Directionlets: anisotropic multidirectional representation with separable filtering. *IEEE Transactions on Image Processing*, 2006, **15**(7): 1916−1933

4 Candés E J. Ridgelets: Theory and Application [Ph. D. dissertation], Stanford University, Stanford CA, 1998

5 Candés E J, Donoho D L. Curvelets — a surprisingly effective nonadaptive representation for objects with edges. *Curves and Surfaces*, Nashville, TN: Vanderbilt University Press, 2000. 105−120

6 Strack J L, Candés E J, Donoho D L. The curvelet transform for image denoising. *IEEE Transactions on Image Processing*, 2002, **11**(6): 670−684

7 Candés E J, Demanet L, Donoho D L, Ying L X. Fast discrete curvelet transforms. *Multiscale Modeling and Simulation*, 2006, **5**(3): 861−899

8 Do M N, Vetterli M. The contourlet transform: an efficient directional multiresolution image representation. *IEEE Transactions on Image Processing*, 2005, **14**(12): 2091−2106

9 Do M N. Directional Multiresolution Image Representations [Ph. D. dissertation], Lausanne Federal Polytechnic School, Lausanne, Swiss, 2001

10 da Cunha A L, Zhou J P, Do M N. The nonsubsampled contourlet transform: theory, design, and applications. *IEEE Transactions on Image Processing*, 2006, **15**(10): 3089−3101

11 Zhou H F, Wang X T, Xu X G. Image denoising using Gaussian scale mixture model in the nonsubsampled contourlet domain. *Journal of Electronics and Information Technology*, 2009, **31**(8): 1796−1800

12 Feng H X, Hou B, Jiao L C, Bu X M. SAR image despeckling based on local Gaussian model and MAP in NSCT domain. *Acta Electronica Sinica*, 2010, **38**(4): 811−816

13 Qu X B, Yan J W, Xiao H Z, Zhu Z Q. Image fusion algorithm based on spatial frequency-motivated pulse coupled neural networks in nonsubsampled contourlet transform domain. *Acta Automatica Sinica*, 2008, **34**(12): 1508−1514

14 Li T J, Wang Y Y. Biological image fusion using a NSCT based variable-weight method. *Information Fusion*, 2011, **12**(2): 85−92

15 Bamberger R H, Smith M J T. A filter bank for the directional decomposition of images: theory and design. *IEEE Transactions on Signal Processing*, 1992, **40**(4): 882−893

16 Chen Y, Adams M D, Lu W S. Design of optimal quincunx filter banks for image coding. *Journal on Advances in Signal Processing*, 2007, 2007: 083858

17 Sweldens W. The lifting scheme: a custom-design construction of biorthogonal wavelets. *Applied and Computational Harmonic Analysis*, 1996, **3**(2): 186−200

18 Tran T D, de Queiroz R L, Nguyen T Q. Linear-phase perfect reconstruction filter bank: lattice structure, design, and application in image coding. *IEEE Transactions on Signal Processing*, 2000, **48**(1): 133−147

19 Portilla J, Strela V, Wainwright M J, Simoncelli E P. Image denoising using scale mixtures of Gaussians in the wavelet domain. *IEEE Transactions on Image Processing*, 2003, **12**(11): 1338−1351

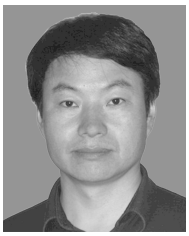

YAN Chun-Man Associate professor at the College of Physics and Electronic Engineering, Northwest Normal University. He received his Ph. D. degree from Xidian University in 2012. His research interest covers MGA theory, image processing, and pattern recognition. Corresponding author of this paper. E-mail: yancha02@163.com

GUO Bao-Long Professor at the Institute of Intelligent Control and Image Engineering (ICIE), Xidian University. He received his bachelor, master, and Ph. D. degrees from Xidian University in 1984, 1988, and 1995, respectively, all in communication and electronic system. His research interest covers neural networks, pattern recognition, intelligent information processing, and image communication.
E-mail: blguo@mail.xidian.edu.cn

YI Meng Ph. D. candidate in circuits and systems, with the Institute of Intelligent Control and Image Engineering, Xidian University. He received his master degree in electrical engineering from Northwestern Polytechnical University in 2008. His research interest covers computer vision and pattern recognition.
E-mail: yimeng@mail.xidian.edu.cn